RESEARCH PAPER

Existence and stability of an intermediate wetting state on circular micropillars

Cheng Luo · Mingming Xiang

Abstract It has been recently reported that, after a liquid drop contacts the bottom of a roughness groove, liquid may not completely fill this roughness groove if the groove is covered with nanostructures. Otherwise, liquid may fill the entire groove. In this work, we explore the reasons behind these phenomena for the case of circular micropillars and derive an angle inequality. We show that if the local contact angles satisfy the angle inequality, a locally stable intermediate wetting state may exist. In this intermediate state, liquid does not completely fill the roughness groove, and air pockets still exist in its bottom corners. When roughness grooves have smooth surfaces, the local contact angles are usually less than 135°, violating the angle inequality. However, the incorporation of nanostructures on the grooves may make local contact angles become above 135°, resulting in the satisfaction of the angle inequality. Therefore, the filling phenomena may be different when the grooves are covered with nanostructures or not. In addition to existing experimental results, the derived angle inequality is also validated by in situ observation of water drops in the pressing tests on circular micropillars with and without the coverage of ZnO wires.

Keywords Transition · Cassie–Baxter state · Wenzel state · Circular micropillars · Intermediate wetting state

C. Luo (✉) · M. Xiang
Department of Mechanical and Aerospace Engineering,
University of Texas at Arlington, 500 W. First Street,
Woolf Hall 215, Arlington, TX 76019, USA
e-mail: chengluo@uta.edu

1 Introduction

As a liquid drop is placed on a rough surface, the wetting may be either in Wenzel (1936) or Cassie and Baxter (1944) state. In the Wenzel state, the drop completely fills roughness grooves, while this is not the case in the Cassie–Baxter state. In the latter state, the drop sits on top of roughness structures. The Wenzel state favors, for example, the creation of a super-wetting surface (McHale et al. 2004; Extrand et al. 2007). In contrast, the Cassie–Baxter state is preferred when a liquid-repellent surface is desired (Neinhuis and Barthlott 1997; Ou et al. 2004). In comparison with Wenzel state, this wetting state reduces the pinning effect on a liquid drop, making the drop much easier to move down from the corresponding surface (Neinhuis and Barthlott 1997; Jung and Bhushan 2008).

A drop may contact the base of a roughness groove due to a large deflection of the drop bottom surface or the depinning of this bottom surface from top edges of rough structures. When this contact occurs, mainly based on experimental observation, it is often considered that the liquid should immediately fill the roughness groove (Extrand 2004; Patankar 2004; Jung and Bhushan 2008; Reyssat et al. 2008; Kusumaatmaja et al. 2008). Subsequently, Cassie–Baxter state is transitioned to that of Wenzel. Accordingly, whether the contact has occurred is employed as a criterion to judge the transition between the two wetting states (Neinhuis and Barthlott 1997; Ou et al. 2004; Extrand 2004; Patankar 2004; Jung and Bhushan 2008; Luo et al. 2011). For simplicity, this transition criterion is called "contact criterion" thereafter. The aforementioned roughness grooves have smooth surfaces. On the other hand, it has been recently reported that, when roughness grooves are covered by nanostructures, such as ZnO wires (Luo et al. 2012; Luo and Xiang 2012) and

silicone nanofilaments (Verho et al. 2012), after water drops contact the corresponding groove bottoms, Cassie–Baxter state does not change to that of Wenzel. Instead, another wetting state may be formed, which is subsequently referred to as "intermediate state." In the intermediate wetting state, water does not completely fill the roughness groove, and air pockets still exist in its bottom corners. Thus, it is interesting to understand why different wetting states may be generated when groove surfaces are covered with and without nanostructures.

Micropillars and microchannels are commonly employed to enhance surface hydrophobicity (Wenzel 1936; Cassie and Baxter 1944; Bico et al. 1999, 2001; Lafuma and Quere 2003; Marmur 2003; He et al. 2003; Extrand 2004; Patankar 2004; Nosonovsky and Bhushan 2007; Jung and Bhushan 2008; Reyssat et al. 2008; Kusumaatmaja et al. 2008; Liu and Luo 2010; Extrand and Moon 2010; Luo et al. 2011; Verho et al. 2012; Qiao et al. 2012). These microstructures normally have vertical sidewalls, instead of inclined ones, since ultra-violet lithography, the most commonly used approach to fabricate micropatterns, employs vertical radiation exposure to transfer patterns. In a previous work (Luo et al. 2012), we explored the applicability of the contact criterion to the case of microchannels. We found that, once an angle inequality is met due to the incorporation of ZnO wires on the inner surfaces of the microchannels, Cassie–Baxter state may be transitioned to intermediate state, instead of that of Wenzel. Also, the intermediate wetting state is locally stable in the sense that its energy state is lower than that of the Wenzel model.

In a follow-up work (Luo and Xiang 2012), we further considered the case of polygonal and circular pillars, and also derived an angle inequality, which is identical to the one derived in the case of microchannels (Luo et al. 2012). In the case of pillars, this angle inequality is a necessary condition that local contact angles and the inclined degree of the pillars should meet for the existence of an intermediate state. As in the case of microchannels, once this inequality is violated, there should not exist any intermediate state, and the contact criterion is also applicable to the case of micropillars. On the other hand, different from that in the case of microchannels, the satisfaction of this inequality does not guarantee the existence of a stable intermediate state for the case of micropillars. For the existence of a stable intermediate state, two conditions should be satisfied. First, there exists an equilibrium state after the contact. Second, there is an energy barrier between this equilibrium state and that of Wenzel. The consideration of these two conditions may give precise bounds of local contact angles and inclined degrees of pillar sidewalls for the existence of a stable intermediate state, which could also be used to identify the exact range

that the contact criterion is applicable. We did so for the case of microchannels (Luo et al. 2012), since the corresponding air/liquid interfaces have simple shapes. However, we did not consider the two conditions in the case of micropillars due to lack of analytical expression of the related air/liquid interfaces (Luo and Xiang 2012). Accordingly, although the derived inequality is identical to the one for the case of channels, it may not give a precise range that the contact criterion is valid.

In this work, using a new approach, we consider the aforementioned two conditions for the case of circular pillars with vertical sidewalls, while the case that circular pillars have concave sidewalls has been reported elsewhere (Luo and Xiang 2013). This approach does not rely on the explicit expression of the interface profile, making it feasible to explore the applicability of the contact criterion. Subsequently, we apply the derived theoretical results to interpret some experimental results shown in both of our previous work (Luo and Xiang 2012) and Verho et al. (2012).

2 Existence of an equilibrium state inside grooves

Assume that there exists an equilibrium state after a liquid drop contacts the base of grooves, which are located between circular micropillars with vertical sidewalls, in a quasi-static manner (Fig. 1). Also assume that the drop profile around the bottom corner of a circular micropillar has an axisymmetric shape. As observed from Fig. 1a, liquid is always considered to be continuous, while the air gaps around pillars may be isolated. Accordingly, the air/liquid interface around a pillar may be isolated. Let a_1b_1 and a_2b_2 represent two of the profile's meridian curves (Fig. 1a). a_1 and a_2 are the triple-phase contact points at the base of the grooves, while b_1 and b_2 are those on the pillar sidewall. Without loss of generalization, only a_1b_1 is considered in the following analysis, and the same analysis also applies to a_2b_2. Set r_0 to be the radius of the pillar. Furthermore, use h_0 to denote the height of the pillar. As already demonstrated before (Luo and Xiang 2012), if h_0 is less than the capillary length of liquid (it is 2.7 mm for water), which is actually the case of this work, then the gravity effect on the drop bottom can be neglected. Accordingly, by Young–Laplace equation (Adamson 1990), liquid pressure inside the bottom portion of a drop is uniform, and

$$p_w - p_a = 2\gamma b, \tag{1a}$$

$$p_w = p_{wt} + \rho g h, \tag{1b}$$

$$\frac{1}{R_1} + \frac{1}{R_2} = 2b, \tag{1c}$$

where p_w and p_a denote liquid pressure and air pressure at a point of a_1b_1, respectively, γ is surface tension of liquid,
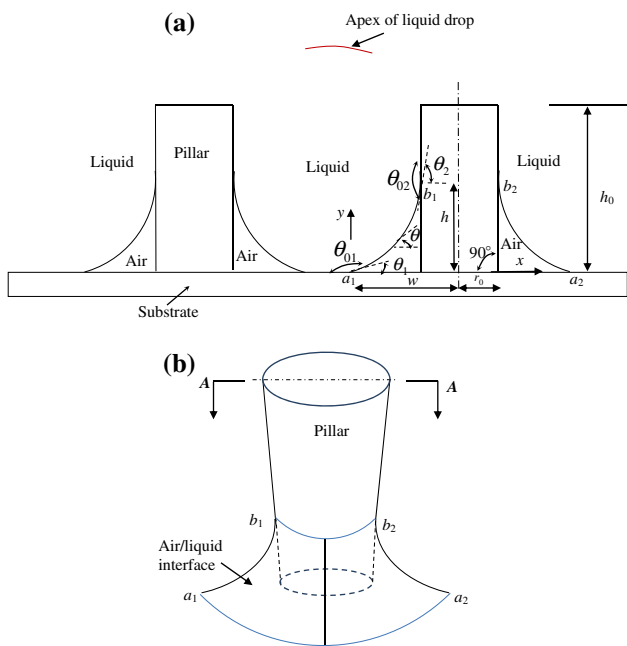
Fig. 1 **a** Cross-sectional profile of the air/liquid interface around the bottom corner of a circular micropillar in a possible intermediate state when a liquid drop contacts the bottoms of the grooves between the micropillars, and **b** perspective view of the air/liquid interface

p_{wt} represents the liquid pressure at the drop apex, ρ is mass density of liquid, g denotes gravitational acceleration, h is the height of the drop, R_1 and R_2 are radii of the maximal and minimal curvatures at this point, respectively, and b represents mean curvature at the point and is constant on the bottom surface of the drop. R_1 and R_2 are considered positive if their associated curves on the liquid surface bend toward air. Further, assume that the drop cap has a convex shape. Then, as also demonstrated before (Luo and Xiang 2012), it follows from Eq. (1c) that b is a positive constant.

Set up an x-y rectangular coordinate system. x and y axes are along horizontal and vertical directions, respectively, and the origin is located at a_1 (Fig. 1a). Set s to be the arc length from a_1 to a point on a_1b_1. Let θ denote the angle formed by the tangent to a_1b_1 and the horizontal direction at a point on this curve. Set θ_1 and θ_2 to be the values of θ at a_1 and b_1, respectively. Equilibrium contact angles on the sidewalls of a micropillar are considered to be the same, while they may be different from the one on the bottom of the micropillar. Let θ_{01} and θ_{02} be equilibrium contact angles on the pillar sidewalls and groove bottoms, respectively. If the micropillar sidewalls and groove bottoms are smooth, then θ_{01} and θ_{02} are intrinsic contact angles. Otherwise, they are apparent contact angles. Furthermore, by geometric analysis, at a_1 and b_1, we have, respectively,

$$\theta_1 = 180^\circ - \theta_{01}, \tag{2a}$$

$$\theta_2 = \theta_{02} - 90^\circ. \tag{2b}$$

Both θ_{01} and θ_{02} are considered to be greater than 90°, i.e., the surfaces of the micropillars and grooves are lyophobic. Subsequently, it follows from Eqs. (2a) and (2b) that

$$0^\circ < \theta_1 < 90^\circ, \tag{3a}$$

$$0^\circ < \theta_2 < 90^\circ. \tag{3b}$$

In the case of circular micropillars, Eq. (1b) can be rewritten in terms of θ and s as

$$\frac{d\theta}{ds} - \frac{\sin\theta}{w - x} = 2b, \tag{4}$$

where w denotes the distance between a_1 and the central axis of the micropillar (Fig. 1a). Equations (2a) and (2b) are also two boundary conditions for Eq. (4). In summary, in order to have an equilibrium state, i.e., to make a_1 stationary, there should exist a solution to Eqs. (4) and (2) under the condition that $b > 0$.

Equation (4) can be further rewritten as

$$\frac{d[(w - x)\sin\theta]}{dx} = 2b(w - x), \tag{5}$$

where $\frac{dx}{ds} = \cos\theta$ was used in deriving this equation from Eq. (4). With the aid of Eq. (2b), it follows from Eq. (5) that

$$\sin\theta = \frac{c}{(w - x)} - b(w - x), \tag{6}$$

where c is a constant and has the following expression:

$$c = r_0 \sin\theta_2 + br_0^2. \tag{7}$$

With the assistance of Eqs. (2a) and (7), it follows from Eq. (6) that

$$b = \frac{r_0 \sin\theta_2 - w \sin\theta_1}{w^2 - r_0^2}. \tag{8}$$

By Eqs. (8), (2a), and (2b), the requirement that $b > 0$ results in

$$\sin\theta_2 > \frac{w}{r_0}\sin\theta_1. \tag{9}$$

Given that Ineq. (9) is met, it follows from Eq. (8) that w is related to r_0, θ_1, θ_2, and b by

$$w = \frac{\sqrt{\sin^2\theta_1 + 4r_0 b \sin\theta_2 + 4r_0^2 b^2} - \sin\theta_1}{2b}. \tag{10}$$

In addition, since

$$\frac{dy}{dx} = \tan\theta, \tag{11}$$

with the assistance of Eq. (6), it follows from Eq. (11) that

$$\frac{dy}{dx} = \frac{c - b(w-x)^2}{\sqrt{\left(1 + \frac{bc}{2}\right)(w-x)^2 - \left[b^2(w-x)^4 + c^2\right]}}. \quad (12)$$

Let x_p and y_p represent x and y coordinates of a representative point p on a_1b_1, where x_p ranges from 0 to $(w - r_0)$. In view of Eq. (12), y_p is given below:

$$y_p(x_p) = \int_0^{x_p} \frac{c - b(w-x)^2}{\sqrt{\left(1 + \frac{bc}{2}\right)(w-x)^2 - \left[b^2(w-x)^4 + c^2\right]}} dx. \quad (13)$$

This equation gives a solution to Eqs. (4) and (2). Its right-hand side is an elliptical integral, which can be numerically integrated. Once θ_1, θ_2, w, and r_0 are given, Eq. (8) gives a unique value to b. Subsequently, a unique value of y_p can be obtained from Eq. (13). Thus, Eq. (13) is also a unique solution to Eqs. (4) and (2). The value of h can also be determined by solving Eq. (13). It equals the value of y_p when $x_p = w - r_0$ and is considered to be less than h_0.

According to the above consideration, for given θ_1, θ_2, w, and r_0, Ineq. (9) is both sufficient and necessary conditions for having a solution to Eqs. (4) and (2). Next, as done in our previous work (Luo and Xiang 2012), we also derive another necessary condition that only involves θ_1 and θ_2.

Substitution of Eq. (6) into Eq. (4) leads to

$$\frac{d\theta}{ds} = b + \frac{c}{(w-x)^2}. \quad (14)$$

Since both c and b are positive by Eq. (14), we have

$$\frac{d\theta}{ds} > 0. \quad (15)$$

This inequality implies that θ increases with increasing s. Hence, we have

$$\theta_2 > \theta_1, \quad (16)$$

which is a necessary condition for the existence of a solution to Eqs. (4) and (2) and which is also identical to the one derived in our previous work for the case of polygonal and circular pillars (Luo and Xiang 2012).

3 Local stability of the intermediate state

In order to make the constructed equilibrium state locally stable, it should be separated from the Wenzel state by an energy barrier. Otherwise, liquid continues to spread on the groove base until the bottom corners of micropillars are completely filled. Subsequently, the wetting state is changed to that of Wenzel, which is the case of our previous report (Luo et al. 2011).
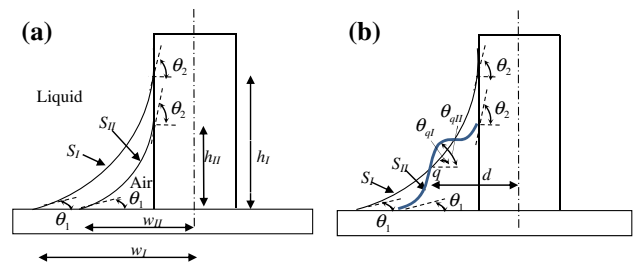

Fig. 2 Schematics of **a** reduction in air gap around the bottom corner of a pillar with the increase in liquid pressure and **b** a possible configuration that S_I intersects with S_{II}

Next, we consider the local stability of the constructed equilibrium state. Differentiation of Eq. (10) with respect to b leads to

$$\frac{dw}{db} = \frac{\sin\theta_1}{2b^2}\left(1 - \frac{\sin\theta_1 + \frac{2r_0 b\sin\theta_2}{\sin\theta_1}}{\sqrt{\sin^2\theta_1 + 4r_0 b\sin\theta_2 + 4r_0^2 b^2}}\right). \quad (17)$$

It can be readily shown that if Ineq. (16) holds true, then

$$\frac{dw}{db} < 0, \quad (18)$$

and vice versa. This inequality indicates that w decreases with the increasing b. Furthermore, based on Leibniz rule (Greenberg 1998), it follows from Eq. (13) that $\frac{dh}{dw} > 0$. This implies that h also decreases with the increasing b. As demonstrated below, in addition to the two end points, other points on a_1b_1 should also move toward the bottom corner of the pillar with the increase in b (Fig. 2a). Let w_I and w_{II} denote the corresponding values of w when b is increased from b_I to b_{II}. Accordingly, we have $w_I > w_{II}$. Use s_I and s_{II} to represent a_1b_1 in these two cases, respectively. Set h_I and h_{II} to be the heights of s_I and s_{II}, separately. Suppose s_I and s_{II} have some intersecting points. According to geometric analysis, under the conditions that $w_I > w_{II}$ and $h_I > h_{II}$, s_I and s_{II} should intersect at least at two points (Fig. 2b). Let q represent one of these intersecting points. Use d to denote the distance between q and the central axis of the pillar. Let θ_{qI} stand for the angle formed by the tangent to s_I and the horizontal direction at q. Set θ_{qII} to be the one subtended by the tangent to s_{II} and the horizontal direction at the same point. Subsequently, according to geometric analysis, we have $\theta_{qI} < \theta_{qII}$ (Fig. 2b). On the other hand, by Eq. (6), we have $\sin\theta_{qI} = \frac{r_0\sin\theta_2 + b_I(r_0^2 - d^2)}{d}$ and $\sin\theta_{qII} = \frac{r_0\sin\theta_2 + b_{II}(r_0^2 - d^2)}{d}$. Since $b_I < b_{II}$ and $d > r_0$, we get $\sin\theta_{qI} > \sin\theta_{qII}$. Accordingly, $\theta_{qI} > \theta_{qII}$, which contradicts with the previous result that $\theta_{qI} < \theta_{qII}$. Therefore, there is no intersecting point between s_I and s_{II}. These results imply (1) the air gap around the

bottom corner of a micropillar decreases with the increase in liquid pressure, and (2) an additional force is needed to increase liquid pressure for reducing this air gap. Thus, if Ineq. (16) is met, then the intermediate state should be separated from that of Wenzel by an energy barrier and vice versa. In this sense, Ineq. (16) is both sufficient and necessary conditions to make the intermediate state locally stable.

4 An inequality to meet

According to the consideration in the previous two sections, for the existence of a locally stable intermediate state, Ineqs. (9) and (16) should both be met. With the aid of Ineqs. (3a) and (3b), it is readily shown that once Ineq. (9) is satisfied, Ineq. (16) is met. On the other hand, when Ineq. (16) holds true, there always exists a w_1, which satisfies the following relation:

$$\frac{\sin \theta_2}{\sin \theta_1} > \frac{w_1}{r_0} > 1. \tag{19}$$

This result ensures that if w falls between r_0 and w_1, then Ineq. (9) is also met, implying that there always exists a region close to the bottom corner of the pillar, in which there exists a locally stable intermediate state.

The air gap around the bottom of a pillar may still be connected to the outside environment, for instance, through the gaps between nanostructures that may be coated on the micropillars. In such a case, the pressure inside the air gap still equals the atmospheric pressure. In case the air gap around the bottom of a pillar is completely isolated from the outside, the pressure in the air gap may increase when the air gap around a pillar is compressed by the liquid drop, while the air pressure on the drop top remains the same. By Eq. (1a), this means that actually a higher liquid pressure is needed to further compress the air drop. This also implies that air pressures around the liquid drop may be different. Subsequently, for a small drop, whose half size is less than the capillary length of the liquid and thus whose gravity effect is neglected, by Eq. (1a) again, the mean curvature around this drop may vary, since the liquid pressure inside the drop is uniform. Therefore, for a liquid drop to be stationary (i.e., at equilibrium), instead of examining the mean curvature, our concern is whether the liquid pressure is balanced inside this drop.

Two points related to the balance of liquid pressure inside a drop can be obtained based on the stability consideration in the previous section. First, for a given w in this region, the corresponding value of b is determined using Eq. (8). When p_w, calculated using Eq. (1a) and this value of b, is larger than the one calculated employing Eq. (1b), which is the liquid pressure at the bottom portion

of the drop, to maintain the pressure balance inside the drop, a_1 moves back toward the center of the groove or the liquid drop loses contact with the bottom of the groove. Second, if the former value of p_w is less than the latter one, then a_1 continues to move toward the corner of the pillar until the two values of p_w are equal. In summary, the satisfaction of Ineq. (16) guarantees the existence of a locally stable intermediate state after a liquid drop contacts the base of grooves.

With the aid of Eq. (2a) and (2b), Ineq. (16) can be rewritten in terms of θ_{01} and θ_{02} as

$$(\theta_{01} + \theta_{02}) > 270^{\circ}. \tag{20}$$

This inequality is identical to the one derived in our previous work for the case that circular pillars have vertical sidewalls (Luo and Xiang 2012). Ineq. (20) was derived in the previous work as a necessary condition for the existence of an intermediate state, while it is also a sufficient condition as shown in this work. Consequently, we have arrived at an angle criterion: once θ_{01} and θ_{02} of circular micropillars with vertical sidewalls satisfy Ineq. (20), there exists a locally stable intermediate wetting state after a liquid drop contacts the base of grooves in a quasi-static manner. This angle criterion is similar to the one that we have previously derived for the case of microchannels (Luo et al. 2012).

A set of values of θ_{01} and θ_{02} may be experimentally measured, depending on the volume of a liquid drop (de Gennes et al. 2004; Marmur 2009). These sets of values vary between receding and advancing angles. Accordingly, the minimum requirement in designing circular pillars for having a locally stable intermediate state is that the advancing angles on the pillar sidewalls and groove bottom should meet Ineq. (20). For the sake of security, it is better to have the receding angles, which are the minimum possible values of θ_{01} and θ_{02} that satisfy this inequality.

5 Experimental validation

5.1 Existing results

In our previous work (Luo and Xiang 2012), we did the pressing tests on six kinds of SU-8 circular micropillars, which all have approximately vertical sidewalls while vary in the pitches or in the local contact angles. On three kinds of these micropillars, groove surfaces were smooth. On a smooth surface, contact angle is normally less than 120° even if this surface is coated with highly water-repellant materials (Lafuma and Quere 2003), such as Teflon. Hence, Ineq. (20) was violated, and water drops collapsed after their contact with the grooves. However, on another three kinds of micropillars, Ineq. (20) was met, since the surfaces of the grooves located between the micropillars were

Fig. 3 **a** Perspective views of SU-8 micropillars. Representative first and second kinds of circular pillars, which were covered with **b** Teflon and **c1** ZnO wires, respectively. **c2** Close-up and **c3** *side views of ZnO wires*. All are scanning electron microscopy (SEM) images
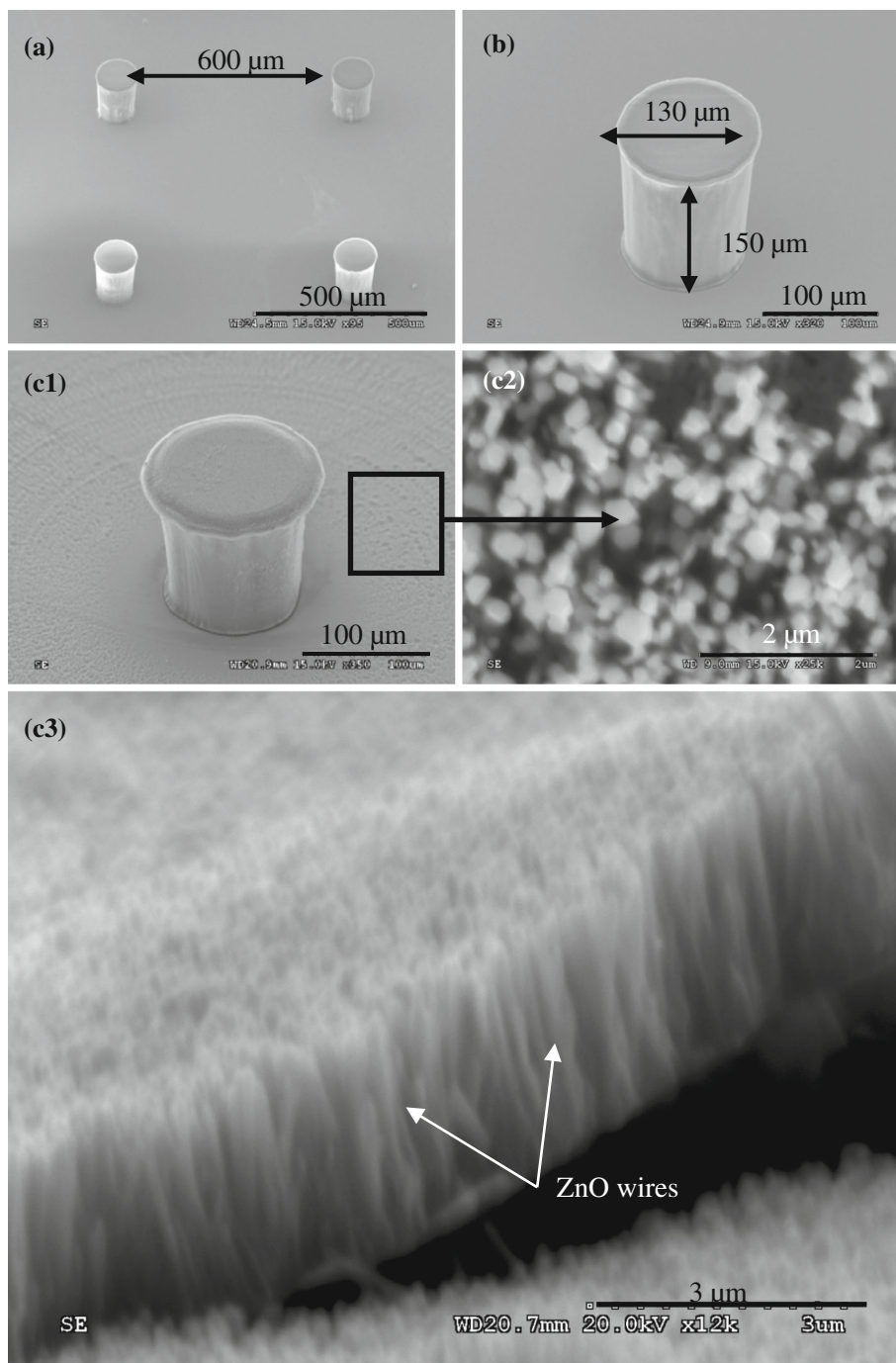
covered with ZnO wires, which made both θ_{01} and θ_{02} above 135°. Consequently, intermediate states were found.

In Verho et al. (2012), two sets of Si circular micropillars with identical dimensions (diameter 10 μm, height 5 or 10 μm, and pitch 20 μm) were examined. The first set was coated with a hydrophobic fluoroalkylsilane monolayer, which had advancing and receding angles of 118° ± 2° and 102° ± 2°, respectively, on flat surfaces. The second set of micropillars was covered with silicone nanofilaments, which made advancing and receding angles become 170° ± 2° and 145° ± 2°, separately, on flat surfaces. Accordingly, Ineq. (20) was violated on the first set of micropillars, while it was met on the second set. Hence, intermediate states existed on the second set of micropillars, while only Wenzel states existed on the first set when water contacted the base of grooves, which were actually the experimental results reported in Verho et al. (2012).
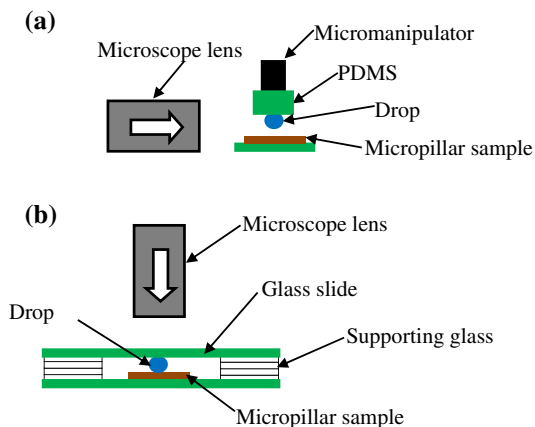
Fig. 4 Setups for **a** first and **b** second types of pressing tests to obtain *side* and *top views* of pressing results, respectively

5.2 New tests

Experiments are also done in this work to have in situ observation of how a_1 moves on the bottom of a groove when water pressure is increased or decreased. In other words, we desire to examine whether, as predicted in Sect. 4, a_1 moves toward or away from the bottom corner of a pillar with the increase or decrease in the water pressure when Ineq. (20) is met. For this purpose, two of the six kinds of SU-8 circular micropillars, which have been previously examined in Luo and Xiang (2012), are adopted in this work (Fig. 3). These two kinds have the largest pitch of 600 μm, which makes it relatively easy to observe the movement of a_1 on the bottom of the gap. They also have

the same radii of 130 μm. On the other hand, to enhance hydrophobicity, the first kind of micropillar is coated with Teflon (Fig. 3b), while the second kind is covered with ZnO wires, which have hexagonal cross-sections with an average height of 2.8 μm and diameters of 0.15–0.36 μm (Fig. 3c). The advancing angles are adopted as the values of θ_{01} and θ_{02}. In the case of the first kind of micropillars, the values of θ_{01} and θ_{02} are both $119° \pm 2°$, while they are both $169° \pm 2°$ for the second kind of micropillars. Accordingly, the values of θ_{01} and θ_{02} for the first kind of micropillars do not meet Ineq. (20), while those for the second kind satisfy this inequality.

Through only side views, due to block of water, it was not clear whether water completely filled the middle grooves after the drops had contacted the bottoms of these grooves (Luo and Xiang 2012). To solve this problem, similar to what was done in Verho et al. (2012), we also take top views of the pressed water drops in this work. Thus, two types of pressing tests are conducted on each kind of SU-8 micropillars. In the first type (Fig. 4a), an optical microscope (mm001300m of Metallurgical microscope Company) is rotated by 90° to have a side view of air/water interfaces between micropillars, and a polydimethylsiloxane (PDMS) plate ($5 \times 5 \times 10$ mm^3) is put on the top of a water drop to slowly press it against micropillars. The vertical movements of this plate are controlled by a micromanipulator (M3301R of World Precision Instruments) with a precision of 100 μm. In the second type of pressing tests (Fig. 4b), a Teflon-coated glass slide ($25 \times 25 \times 1$ mm^3) is placed on a water drop,

Fig. 5 Pressing test results on the first kind of micropillars. In order to get a better understanding of these results, **a** side and **b** top views are placed together, while they were taken in the first and second pressing tests, respectively. The corresponding area of *top views* is *boxed* in **a1**. **a1, b1** Before and **a2, b2** after the contact of water with the base of grooves. **a3, b3** Water residue on the sample after the pressing slide has been removed. The *scale bars* represent 420 μm
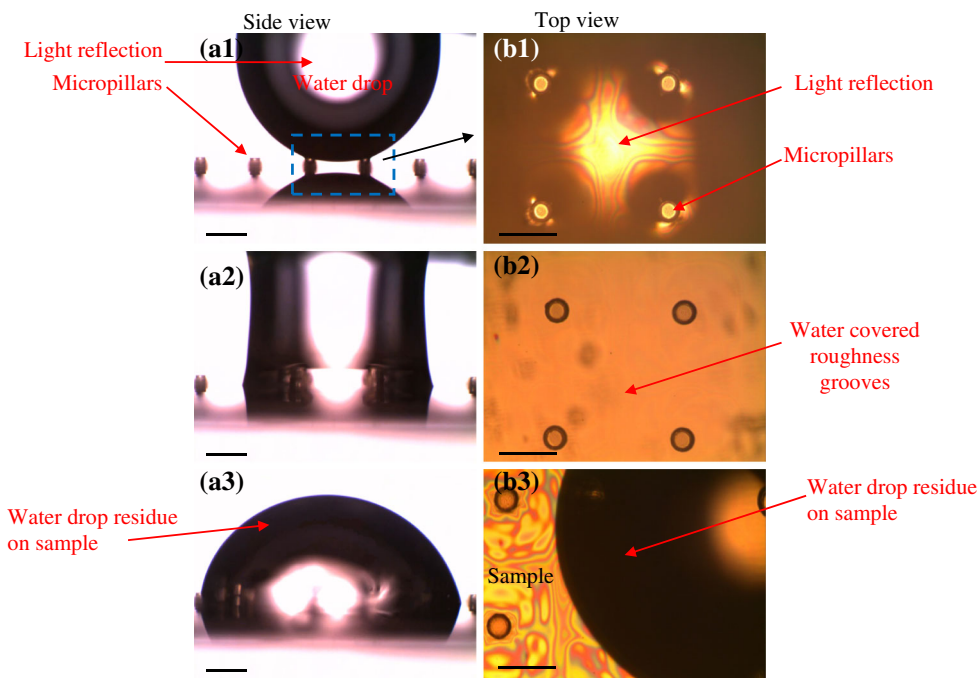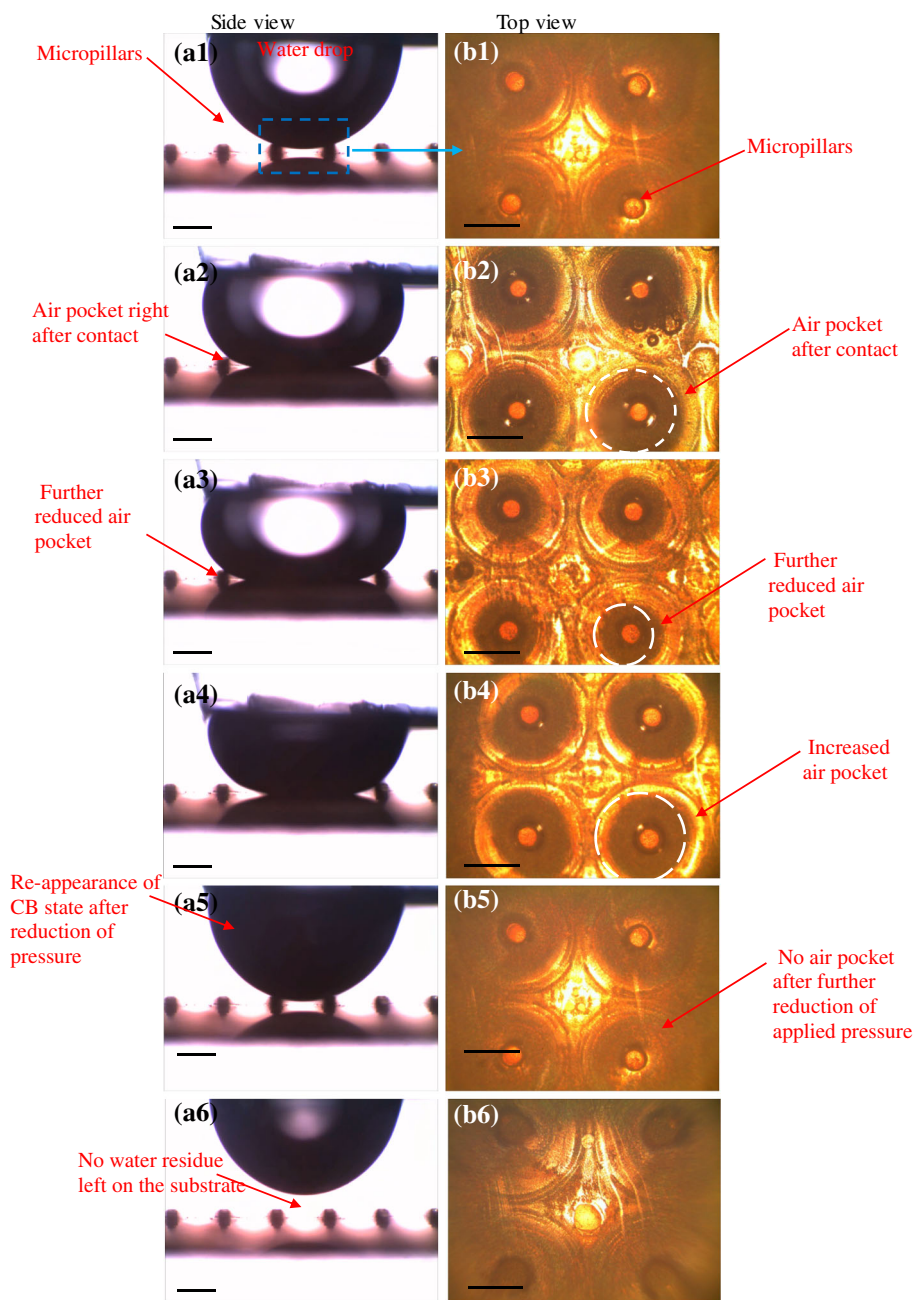
Fig. 6 a, b *Side* and *top views* of pressing test results on the second kind of micropillars. The corresponding area of *top views* is *boxed* in **a1**. **a1–a4** and **b1–b4** increase, and **a5–a7** and **b5–b7** reduce applied pressure. The *scale bars* represent 420 μm

and the optical microscope is used to observe the air/water interface from the top. Thinner glass slides (25 × 25 × 0.2 mm³) are stacked together to serve as the supporters of the Teflon-coated glass slide. This glass slide can be lowered down or lifted up with a precision of 200 μm (which is the thickness of a thinner glass slide) to increase or decrease the applied pressure on the water drop by removing or adding thinner glass slides in the supporters. Small water drops are used in the pressing tests, and their volumes range from 6 to 9 μl. Such a drop has a spherical cap after it is placed on the substrate.

An important point was observed through pressing tests on the first kind of micropillars (Fig. 5). After water drop had contacted the bottom of a groove, it collapsed, and water completely covered the bottom corners of the outside pillars underneath this water drop. Also, the increase or decrease in the applied pressure caused the increase or decrease in the number of the pillars covered by the water drop. The air gaps surrounding middle pillars could be clearly identified through top views according to the light reflection (see, for example, Figs. 5b1, 6b). The bottom corners of the outside pillars underneath the drop were

completely covered by water according to the side view (Fig. 5a2), while the bottom corners of the middle pillars were completely covered by water based on the top view (Fig. 5b2). In addition, part of the water drop was left on the substrate when the pressing plate was removed (Fig. 5a3, b3), implying that Wenzel state was not completely transited back to that of Cassie–Baxter.

On the other hand, different results were observed on the second kind of micropillars (Fig. 6). After water had contact with the base of a few grooves, the air pockets could be observed around the outside micropillars through side views (Fig. 6a2–a4). Furthermore, through top views, we could clearly see that air pockets around the middle pillars increased or decreased the sizes with the decrease or increase in water pressure (Fig. 6b2–b4), which were invisible in the side views due to the block of water. Eventually, the water drop recovered its Cassie–Baxter wetting state after much reduction in the applied pressure (Fig. 6a5, b5). Finally, this water drop was removed from its substrate by the pressing plate or slide, and no water residue was observed on the substrate (Fig. 6a6, b6). In addition, as marked in Fig. 6b, during the processes of increasing and reducing the applied pressure, the air pocket had an approximately circular contact area with the base of grooves, partially supporting our previous assumption that the liquid/air profile has an axisymmetric shape.

Two points can be summarized from the pressing results on the two kinds of micropillars. First, as predicted using Ineq. (20), intermediate states exist on the second kind of micropillars, but not on the first kind. Second, the experimental results on the second kind of micropillars clearly demonstrate that, as predicted in Sect. 4, a_1 moves toward or away from the bottom corner of a pillar with the increase or decrease in the water pressure when Ineq. (20) is met.

Due to lack of simple expression of the air/liquid interface, we do not estimate the energy barrier that separates the intermediate state and the Wenzel model. On the other hand, as commented in Luo and Xiang (2012), when the applied pressure is high enough to make water penetrate and fill the valleys between the coated ZnO wires on the second kind of micropillars, the corresponding values of θ_{01} and θ_{02} may be reduced, leading to the violation of Ineq (20) and causing the transition from the intermediate state to that of Wenzel.

6 Summary and conclusions

In this work, we derive an angle inequality, which is Ineq. (20), to examine whether the contact criterion is applicable to the case of circular micropillars and also to understand why the coverage of nanostructures on the corresponding groove surfaces may result in an intermediate wetting state

after a liquid drop contacts the groove bottom. We directly observed the evolution of air/water interfaces around micropillars through the front and top views when applying pressure on the water drop. By considering the existence and stability of an equilibrium state, we demonstrate (1) when this angle inequality is met due to the increase of local contact angles by, for example, nanostructures, there exists a locally stable intermediate state after a water drop contacts the base of grooves in a quasi-static manner and the contact criterion does not hold for the corresponding micropillars, and (2) if the inequality is violated, then such an intermediate state does not exist and the contact criterion holds true.

References

Adamson AV (1990) Physical chemistry of surfaces, 5th edn. Wiley, New York

Bico J, Marzolin C, Quere D (1999) Pearl drops. Europhys Lett 47(2):220–226

Bico J, Tordeux C, Quere D (2001) Rough wetting. Europhys Lett 55(2):214–220

Cassie ABD, Baxter S (1944) Wettability of porous surfaces. Trans Faraday Soc 40:0546–0550

de Gennes P-G, Brochard-Wyart F, Quéré D (2004) Capillarity and wetting phenomena: drops, bubbles, pearls, waves. Springer, NY

Extrand CW (2004) Criteria for ultralyophobic surfaces. Langmuir 20(12):5013–5018

Extrand CW, Moon SI (2010) Contact angles of liquid drops on super hydrophobic surfaces: understanding the role of flattening of drops by gravity. Langmuir 26(22):17090–17099

Extrand CW, Moon SI, Hall P, Schmidt D (2007) Superwetting of structured surfaces. Langmuir 23(17):8882–8890

Greenberg MD (1998) Advanced engineering mathematics, 2nd edn. Prentice-Hall, Upper Saddle River, NJ

He B, Patankar NA, Lee J (2003) Multiple equilibrium droplet shapes and design criterion for rough hydrophobic surfaces. Langmuir 19(12):4999–5003

Jung YC, Bhushan B (2008) Wetting behaviour during evaporation and condensation of water microdroplets on superhydrophobic patterned surfaces. J Microsc 229(1):127–140

Kusumaatmaja H, Blow ML, Dupuis A, Yeomans JM (2008) The collapse transition on superhydrophobic surfaces. Europhys Lett 81(3):36003

Lafuma A, Quere D (2003) Superhydrophobic states. Nat Mater 2(7):457–460

Liu XC, Luo C (2010) Fabrication of super-hydrophobic channels. J Micromech Microeng 20(2):025029

Luo C, Xiang MM (2012) Angle inequality for judging the transition from Cassie–Baxter to Wenzel states when a water drop contacts bottoms of grooves between micropillars. Langmuir 28(38):13636–13642

Luo C, Xiang MM (2013) Wetting states on circular micropillars with convex sidewalls after liquids contact groove base. Langmuir 29(48):15065–15075

Luo C, Xiang MM, Liu XC, Wang H (2011) Transition from Cassie–Baxter to Wenzel States on microline-formed PDMS surfaces

induced by evaporation or pressing of water droplets. Microfluid Nanofluid 10(4):831–842

Luo C, Xiang MM, Heng X (2012) A stable intermediate wetting state after a water drop contacts the bottom of a microchannel or is placed on a single corner. Langmuir 28(25):9554–9561

Marmur A (2003) Wetting on hydrophobic rough surfaces: to be heterogeneous or not to be? Langmuir 19(20):8343–8348

Marmur A (2009) Solid-surface characterization by wetting. Annu Rev Mater Res 39:473–489

McHale G, Shirtcliffe NJ, Aqil S, Perry CC, Newton MI (2004) Topography driven spreading. Phys Rev Lett 93(3):036102

Neinhuis C, Barthlott W (1997) Characterization and distribution of water-repellent, self-cleaning plant surfaces. Ann Bot 79(6): 667–677

Nosonovsky M, Bhushan B (2007) Hierarchical roughness optimization for biomimetic superhydrophobic surfaces. Ultramicroscopy 107(10–11):969–979

Ou J, Perot B, Rothstein JP (2004) Laminar drag reduction in microchannels using ultrahydrophobic surfaces. Phys Fluids 16(12):4635–4643. doi:10.1063/1.1812011

Patankar NA (2004) Transition between superhydrophobic states on rough surfaces. Langmuir 20(17):7097–7102

Qiao L, Xiang MM, Luo C (2012) Increase buoyancy of a solid fragment using micropillars. Sens Actuators A Phys 182:136–145

Reyssat M, Yeomans JM, Quere D (2008) Impalement of fakir drops. Europhys Lett 81(2):26006

Verho T, Korhonen JT, Sainiemi L, Jokinen V, Bower C, Franze K, Franssila S, Andrew P, Ikkala O, Ras RHA (2012) Reversible switching between superhydrophobic states on a hierarchically structured surface. Proc Natl Acad Sci USA 109(26): 10210–10213

Wenzel RN (1936) Resistance of solid surfaces to wetting by water. Ind Eng Chem 28:988–994